China Ocean Eng., 2018, Vol. 32, No. 5, P. 614–623
DOI: https://doi.org/10.1007/s13344-018-0063-4, ISSN 0890-5487
http://www.chinaoceanengin.cn/ E-mail: coe@nhri.cn

Analysis on Link Between the Macroscopic and Microscopic Air–Water Properties in Self-Aerated Flows

WEI Wang-ru, XU Wei-lin, DENG Jun*, TIAN Zhong, ZHANG Fa-xing

State Key Laboratory of Hydraulics and Mountain River Engineering, Sichuan University, Chengdu 610065, China

Received February 23, 2018; revised May 10, 2018; accepted June 6, 2018

©2018 Chinese Ocean Engineering Society and Springer-Verlag GmbH Germany, part of Springer Nature

Abstract

Self-aeration in high-speed free surface flows occurs commonly and is of interest to ocean engineering, hydraulic engineering, and environmental engineering. For two-phase air–water flows, macroscopic air–water flow properties develop gradually, accompanied by the change of microscopic air–water structures. In this article, representational experimental studies on macroscopic and microscopic characteristics of self-aerated open-channel flows are summarized and compared. The isolated effect of the flow Reynolds number and air quantity on the differences in air count rate and chord size are analyzed and discussed. The results show that the characterized flow depth y_{50}, affected by the turbulence transfer, is a specific criterion to distinguish the interior air–water structure development. Two distinct linear trends of self-aeration are found, depending on the y_{50}/y_{90} variation with a breaking point at C_{mean} = 0.50. The air count rate and size scale in self-aerated flows are affected by the air quantity of self-aerated flows, even with identical flow Reynolds numbers. Thus, a specific parameter is proposed to assess the air–water structures and a series of self-similarity relationships in self-aeration properties are obtained. The link between macroscopic and microscopic air–water properties results in significant scale effect on air–water structures in self-aerated flows.

Key words: self-aeration, two-phase flows, air concentration, air bubble, open channel

Citation: Wei, W. R., Xu, W. L., Deng, J., Tian, Z., Zhang, F. X., 2018. Analysis on link between the macroscopic and microscopic air–water properties in self-aerated flows. China Ocean Eng., 32(5): 614–623, doi: https://doi.org/10.1007/s13344-018-0063-4

1 Introduction

Self-aeration is a natural phenomenon in high-speed free surface flows, characterized by a substantial amount of air entrainment and strong air–water mixing. As the recognition of air–water flow in open channels develops, self-aeration should be described in macroscopic and microscopic scales. For macroscopic description, the air entrainment process includes aeration inception and mixture depth affecting the structure designs (Hall, 1943; Ferrando and Rico, 2002; Takahashi and Ohtsu, 2012) and air concentration affecting cavitation erosion protection (Rutschmann and Hager, 1990). For microscopic description, the self-aeration results in a series of tiny-scaled air–water structures. Air-phase size and air–water transfer have been recognized for their properties of atmospheric gas transfer (Gulliver and Rindels, 1993; Chanson, 2007, 2013) and mechanism of cavitation prevention (Russell and Sheehan, 1974; Wu et al., 2017), which is of interest to ocean engineering, hydraulic engineering, and environmental engineering.

The total air–water mixture depth and mean air concentration of self-aerated flow have been considered as two important parameters to describe the entire self-aeration development (Wood, 1983; Hager, 1991; Afshar et al., 1994; Wei et al., 2016). The self-aerated flow depth, usually defined by the elevation where local concentration is 0.90, represents the upper boundary of macroscopic air–water mixture, and the mean air concentration at the cross-section represents the aeration development level. However, whether there is a characterized flow depth or another parameter to distinguish the air–water structure difference in the interior of self-aerated flow is not clear, so this should be further studied to gain deep insight into natural air–water flows.

Moreover, differences in microscopic air–water structures for different macroscopic air–water flow conditions are unavoidable (Heller, 2011; Schultz and Flack, 2013). This is more distinct for self-aeration, owing to the air entrainment process through the turbulent free surface (Volkart, 1980; Cain and Wood, 1981; Brocchini and Peregrine, 2001a, 2001b). For example, air bubble count rate and chord length distribution in high and low aerated regions at the mixture flow cross-section are remarkably different (Deng et al., 2015). Specific descriptions of self-aerated

Foundation item: This study was financially supported by the National Key Research and Development Program of China (Grant No. 2016YFC0401901) and the National Natural Science Foundation of China (Grant Nos. 51379138 and 51609162).
*Corresponding author. E-mail: djhao2002@scu.edu.cn

flows have been proposed involving entrapped air in the distorted free surface flowing over the entrained air bubble flow region at the mixture flow cross-section (Wilhelms, 1997; Chanson, 2002; Wilhelms and Gulliver, 2005). Felder and Chanson (2016) discussed the specific air–water properties in local region, where the air concentration is 0.50 of high-speed free surface flows over a stepped spillway, showing the effect of macroscopic free surface scale on the detailed air–water structures. Valero and Bung (2018) theoretically analyzed the relationship between microscopic free surface structure and macroscopic self-aeration occurrence. These investigations indicated that macroscopic air concentrations may correspond to different microscopic air–water structures. However, the recognition of variations in microscopic air–water structure in self-aerated flows is limited. Whether the air–water structures are identical for the same macroscopic condition is still not clear. A lack of information on the comparison of microscopic air–water structures is the main constraint for better understanding the relationship between macroscopic and microscopic air–water characteristics in high-speed self-aerated flows.

The objective of this research is to improve the insight of microscopic interior links in self-aerated flows. A systematic comparison of air concentration variations based on a series of representational studies is conducted, and a characterized flow depth to distinguish the interior air–water structures is proposed. Its relationship with macroscopic parameters is analyzed within different self-aeration development levels. Furthermore, the isolated effects of the flow Reynolds number and air quantity on the differences in air count rate and chord size are analyzed and discussed. A new parameter for the determination of microscopic air–water structures is provided.

2 Flow conditions

In past decades, a number of test measurements for self-aeration in high-speed open-channel flows have been conducted. Table 1 summarizes representational studies on self-aerated open-channel flows, including physical models and prototype tests, considering both self-aeration developing and equilibrium states. This research was conducted in different periods, and the data were obtained by different measuring techniques, including electrical conductivity probes and phase detection intrusive probes. Although different techniques have some differences in the measuring process, such as the calibration of the electrical conductivity probe, the tip sensor size of the phase detection probe, the sampling rate, and the sampling duration, the basic theory for air–water property measurement is the same and is based on the signal variation between the air–water mixture and clear water. Thus, the effect of different measurement techniques on the analysis results can be neglected.

In the present study, the following definitions have been used for local air concentration, air–water flow depth, cross-sectional mean air concentration, air count rate, and air chord length. The local air concentration C is defined as the volume of air per unit volume. The air–water flow depth y_{90} is defined as the elevation where $C = 0.90$. The air concentration gradient k at the flow depth direction is defined as:

$$k = \frac{\mathrm{d}C}{\mathrm{d}(y/y_{90})}. \tag{1}$$

The cross-sectional mean air concentration C_{mean} is defined as (Hager, 1991):

$$C_{\mathrm{mean}} = \frac{1}{y_{90}} \int_{y=y_{90}}^{y=0} C(y)\mathrm{d}y. \tag{2}$$

The air quantity q_a is defined as the air discharge per unit width, deduced from $q_a = q_w \cdot C_{\mathrm{mean}}/(1-C_{\mathrm{mean}})$. Air count rate F is defined as the number of "air volume" per second, where the air volume is considered as a unit air body surrounded by two continuous air–water interfaces (Deng et al., 2015). The air chord length of each air volume d is the length of the straight distance between the two-continuous air–water interfaces. The mean air chord length d_{mean} is

Table 1 Hydraulic conditions for self-aerated flows

References	q_w (m^2/s)	α	Re	Aeration state	Comments
Anderson (1955)	0.2–0.6	15°–45°	Re>1.7×10^5	Developing	Models, electrical conductivity probe. Air concentration.
Straub and Anderson (1958)	0.1–0.9	7.5°–75°	Re>1.2×10^5	Developing & equilibrium	Models, electrical conductivity probe. Air concentration.
Killen (1968)	0.4–0.9	30°–52.5°	Re>3.5×10^5	Developing	Models, electrical conductivity probe. Air concentration.
Cain (1978)	2.2–3.2	45°	Re>1.7×10^6	Developing	Prototype, phase detection intrusive probe. Air concentration.
Xi (1988)	0.2	52.5°	Re>2.4×10^5	Developing	Models, phase detection intrusive probe. Air concentration.
Chanson (1995)	0.15	4°	Re>1.1×10^5	Developing & equilibrium	Models, phase detection intrusive probe. Air concentration.
Chanson and Cummings (1995)	0.15	4°	Re>1.1×10^5	Developing &equilibrium	Models, phase detection intrusive probe. Air concentration, air chord length, air count rate.
Zhang et al. (2008)	0.4–0.8	45°	Re>2.6×10^5	Developing	Models, phase detection intrusive probe. Air concentration, air chord length, air count rate.
Wei (2015)	0.2–0.8	9.5°–28°	Re>1.3×10^5	Developing	Models, phase detection intrusive probe. Air concentration, air chord length, air count rate.

defined as:

$$d_{\text{mean}} = \sum_{i=1}^{N} n_i d_i \Big/ \sum_{i=1}^{N} n_i, \tag{3}$$

where N is the total conducted air count and n_i is the air volume count with a chord size d_i. These studies included wide ranges of flow discharge per unit width q_w, channel slope α, and flow Reynolds number $Re = V \cdot y_{90}/\nu$, where V is the flow velocity and ν is the kinematic viscosity. Based on previous studies (Boes and Hager, 2003; Pfister and Chanson, 2014), scale effects related to air concentrations are small when $Re > (1.0–1.5)\times10^5$, whereas microscopic entrained air properties and diffusion process are likely to be more affected by scale effects. The present analyses respected these limitations and focused on the self-similarities between macroscopic and microscopic air–water properties; thus, these scale effects on air concentration were small and could be expanded to a wide application.

3 Air concentration gradient distribution

In high-speed open-channel flows, when self-aeration occurs at the inception point, air will be entrained through the free surface and diffused into water flow under flow turbulent effect. A continuous air concentration profile forms, varying from clear water to free surface. When fully self-aerated flow generates, air bubbles will reach the near-wall area of the channel bottom without clear water in the entire flow cross-section. In the interior of the self-aerated flow, complicated air–water mixture structures exist, including individual droplets and air bubbles, air–water mixture foams and contorted free surfaces, distributing in different aerated areas of the cross-section. Because of different types of air–water structures, a maximum value of air concentration gradient k_m exists in the middle of the mixture flow cross-sections, as shown in Fig. 1. The value of air concentration gradient k decreases from the peak point k_m to both the free surface and the clear water or the bottom wall. The previous "layered description" is based on the mathematical difference (Straub and Anderson, 1958; Wu, 1988), and the flow depth where k_m exists is considered the "transition depth, " which is an artificial transition plane separating the entire self-aerated region into a high aerated region and a

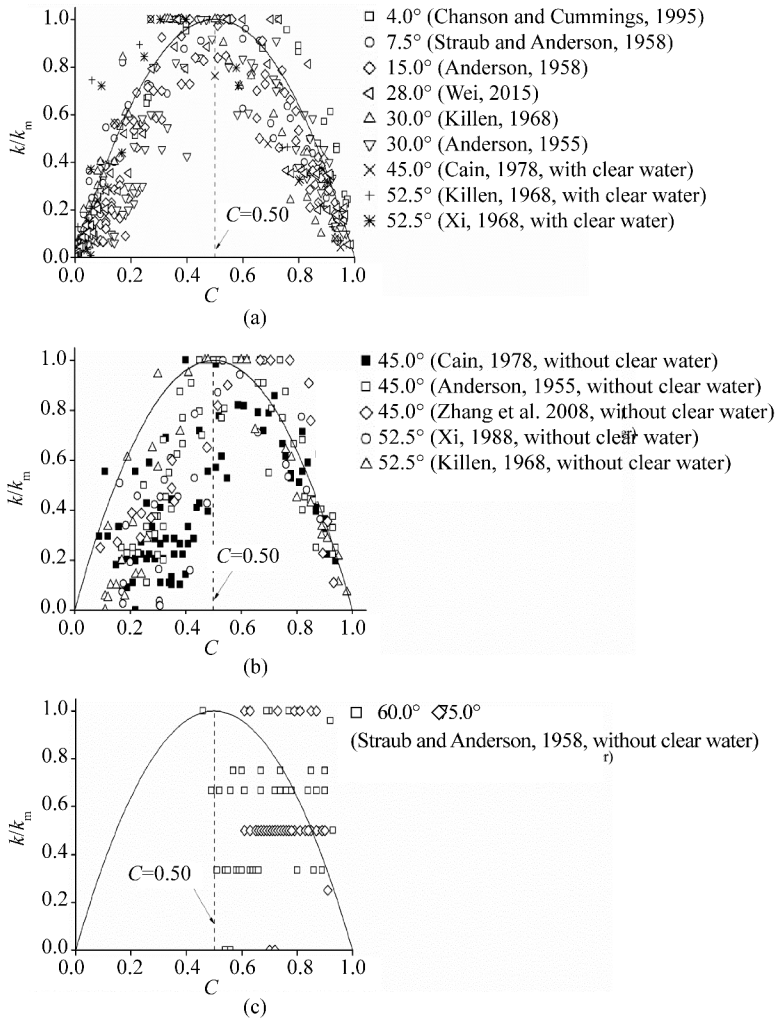

Fig. 1. Distributions of air concentration gradient in self-aerated region.

low aerated region.

Based on the measured data analysis, the distribution of the air concentration gradient is obviously different for different channel slopes and aeration conditions. First, in Fig. 1a, when channel slope α<30°, or α>30° with clear water existence, k_m locates around the flow depth where the air concentration is 0.50, and the distribution profile of the air concentration gradient is symmetrical as a parabolic shape with C = 0.50, approximately presented as the solid line: $k/k_m = 1–4(C–0.5)^2$. In Fig. 1b, for 45°<α<60° without clear water existence, the distribution profile of air concentration gradient becomes asymmetrical. According to the relative positions of data against parabolic line, the difference occurs both in the low- and the high aerated regions. k_m locates in the high aerated region, where C>0.50. This indicates that the self-aeration development level improves in a steeper channel, and the air concentration gradient is reduced in a low aerated region and raised in a high aerated region. When the mixture of air–water flow becomes more uniform, with α = 60°–75°, as shown in Fig. 1c, the distribution profile of air concentration will be mainly in the highly aerated region where no C = 0.50 exists, and k_m locates mainly in the spray and free-surface area, where C = 0.70–0.90 (Felder and Chanson, 2017). In this situation, there is no obvious trend of air concentration gradient, indicating that air–water mixture is highly uniform. This variation of distribution shape confirms the effect of the air–water structure on the bubble frequency distribution analysis by Toombes and Chanson (2007). They showed that the distribution of the air bubble count rate in high and low self-aerated regions may exhibit an asymmetrical quasi parabolic curve, which is affected by the microscopic air–water length scale.

In previous studies about air–water structures in self-aerated flows (Wilhelms and Gulliver, 2005; Killen, 1968), the detailed data showed a remarkable difference in entrained bubbles and entrapped air between high- and low-aeration regions. The depth y_{50} where C = 0.50 is a specific flow depth, representing the interior characteristics of the air–water structure distribution. When the y_{50} existed in the flow cross-section, the difference of the air concentration gradient profile remains between the high and low aeration regions, even for the steep channel slope (α = 52.5°) and high-aeration (C_{mean}>0.50) situations. Moreover, if the position of k_m is the transition depth from the individual bubble flow to the large and complicated air–water structure mixture region, it changes from y_{50} to a highly aerated area where C = 0.50–0.80, which indicates that the difference of the air–water structure develops from the flow interior to the free surface area. The bubble flow region gradually expands to the entire mixture flow cross-section, even in high aerated region.

In Fig. 2, y_{50} shows a good self-similarity relationship with the macroscopic mixture flow depth y_{90}. For C_{mean}<0.50, the value of y_{50}/y_{90} decreases linearly with the increase of C_{mean}, while it follows a different constant decay trend for C_{mean}>0.50. Altogether, the tested data fits are

$$\frac{y_{50}}{y_{90}} = 1.0 - 0.8C_{mean}, \quad 0.00 \leqslant C_{mean} \leqslant 0.50; \tag{4}$$

$$\frac{y_{50}}{y_{90}} = 2.1 - 3.0C_{mean}, \quad 0.50 \leqslant C_{mean} \leqslant 0.70. \tag{5}$$

Furthermore, y_{50}/y_{90} is affected significantly by aeration level, independent of channel slope, developing and equilibrium aeration level. According to the data analysis on the high-aeration conditions, the specific location of y_{50} will not exist in the cross-section of self-aerated flows when C_{mean} exceeds approximately 0.70. The decay trend of y_{50}/y_{90} shows the process of air bubble interior diffusion with the improvement of self-aeration development. For C_{mean}>0.50, local air concentration near the channel bottom was usually larger than 0.30–0.40. This indicates that the air–water mixture develops more uniformly and rapidly, resulting in a difference of the decay trend with large absolute value of gradient.

Based on the basic studies, the y_{50} is the characterized flow depth, representing the development of the interior air–water mixture. By combining the parameters y_{90} and y_0 (where the bottom of the self-aerated region locates), which represent the macroscopic air–water mixture process, the air entrainment downstream of the inception of self-aeration can be classified into three general aerated zones, as shown in Fig. 3, including the following:

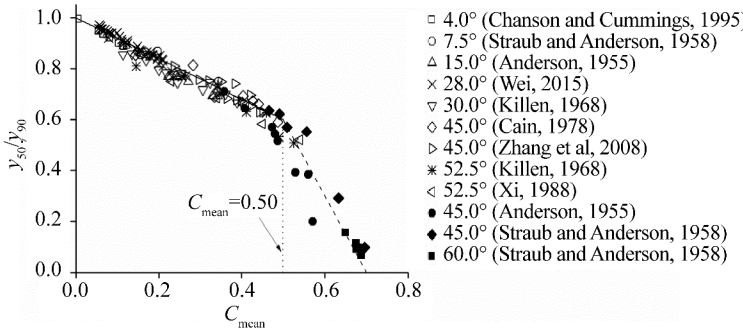

Fig. 2. y_{50}/y_{90} with increasing trend of C_{mean}.

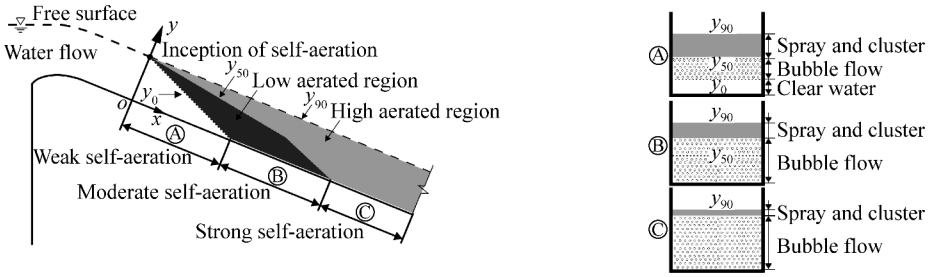

Fig. 3. Sketch of three general self-aeration zones.

Zone A: weak self-aeration zone where $y_0 \neq 0$

Zone B: moderate self-aeration zone where $y_0 = 0$ and $y_{50} \neq 0$;

Zone C: strong self-aeration zone where $y_{50} = 0$.

In Zones A and B, both high and low self-aeration regions exist in the entire flow cross-section, and the difference of air–water structures remains, resulting in variation of the air concentration gradient. The uniform gradient distribution in Zone C shows that the difference of the air–water structure is relatively small. More detailed measurements and verification are needed in the future because of the limited data on air–water structures in Zone C. The detailed analysis on the air–water structure in Zones A and B will be conducted in the following sections.

4 Differences in air count rate and size

4.1 Effects of flow Reynolds number and air quantity

Experimental data from Wei (2015) contained a series of systemic air–water properties in self-aerated flows, including macroscopic air concentration distributions, air–water mixture flow depths, and microscopic air count rate and chord length in the self-aerated region. Thus, these data can be used to analyze the microscopic air–water structures affected by macroscopic air–water flows. The effects of the mixture flow Reynolds number Re and air quantity q_a on the air count rate variation are shown in Fig. 4. For an approximately identical cross-sectional mean air concentration C_{mean}, the air count rate is higher for a larger Re and q_a. The difference is more obvious in the moderately aerated region ($0.2<C<0.8$), where both large and small scaled air–water structures exist. This implies that the fragment and mixture of uniform air–water flow are more developed for higher Reynolds number and larger air quantity for identical local air concentrations.

The differences in the air chord length distribution affected by Re and q_a are depicted in Fig. 5 and Fig. 6, re-

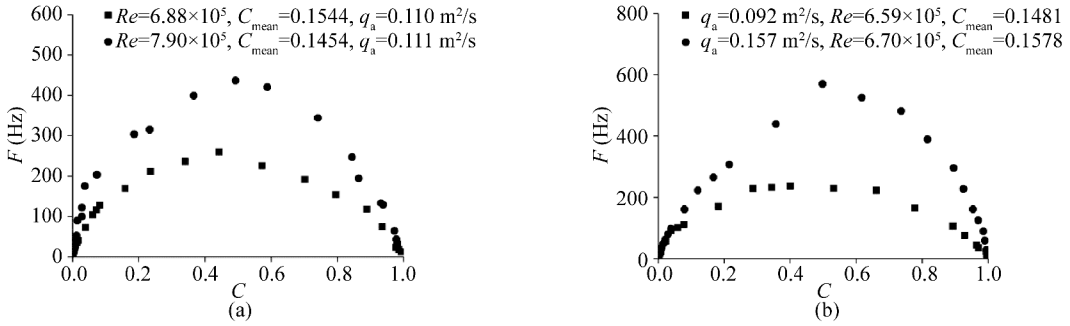

Fig. 4. Effects of (a) Re and (b) q_a on the relationship between air count rate and air concentration.

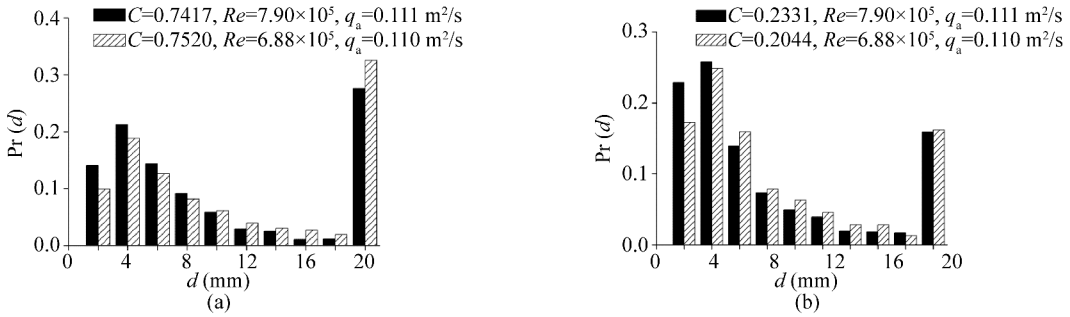

Fig. 5. Effect of Re on air chord length probability distribution in (a) high and (b) low self-aerated areas.

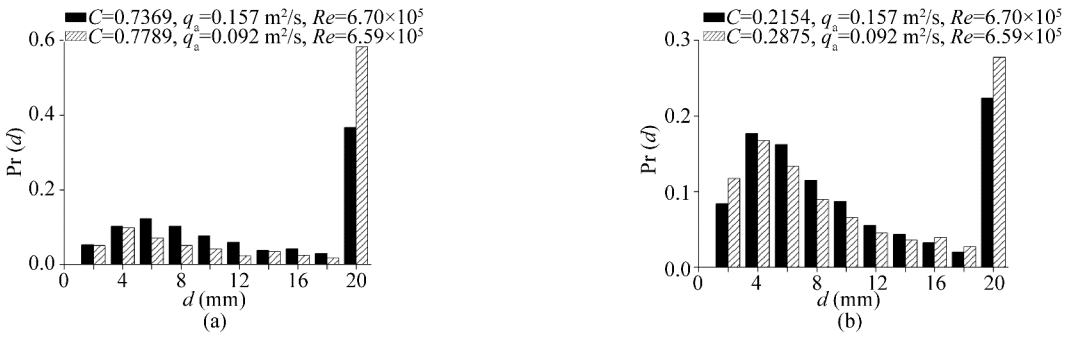

Fig. 6. Effect of q_a on air chord length probability distribution in (a) high and (b) low self-aerated areas.

spectively. Each histogram column represents the count proportion of air chord length in a d-interval. The count proportion of the air chord length, 6–8 mm, is the column labeled 8 mm, and the column labeled 20 mm represents the count proportion for an air chord length larger than 20 mm. First, the count proportion in the small air chord length range (d <6–8 mm) is higher for a larger Re. With the increase of air chord class in the abscissa, the proportion preponderance for larger Re declines gradually, exceeded by the count proportion for a lower Re condition in the large air chord length range. In terms of air quantity effect, the count proportion in the small air chord length range is relatively preponderant for larger q_a. Besides, large scale air–water structure plays an important role in the mixture flow, and the proportion for air chord lengths larger than 20 mm is larger than 20%–30%, even when the local air concentration is relatively low (C = 0.20–0.30).

The distributions of the mean air chord length d_{mean} in the self-aerated region affected by Re and q_a are shown in Fig. 7. Larger Re and q_a result in a decrease in both d_{mean} value and distribution range. In the low aeration region (where C<0.50), the range of d_{mean} reduces from 0<d_{mean}< 20 mm to 0<d_{mean}<10 mm, with the increase Re and q_a. In the highly aerated region (where C>0.50), the range reduces from 20<d_{mean}<100 mm to 20<d_{mean}<60 mm. The decrease of d_{mean} contributes to the entire mixture uniformity and the presence of air in the form of smaller air–water structures. This demonstrates that both the entire flow Reynolds number and the remaining capacity of air quantity influence the microscopic air–water structure scales.

4.2 Relationship between flow conditions and bubble properties

Because of the coupling positive effect of Re and q_a on improving the air–water mixture fragmentation, a dimensionless coefficient K, defined as:

$$K = \frac{Re \cdot q_a}{v} \tag{6}$$

is proposed for the integration description of microscopic air–water structure difference. In Fig. 8, assuming that the ratio of d_{mean}/y_{90} represents the fragmentation level of the entire self-aerated flow, with the increase in K, the value of d_{mean}/y_{90} decreases in both high and low aeration regions, indicating that the size scale of the conveyed air in the self-aerated region is much smaller. As the presence of air bubbles can improve the flow turbulence level (Wang et al., 1990), the part of q_a/v in Eq. (6) can be considered as the ratio of the inertia and viscosity, which is the "additional" specific "air flow" turbulent effect. Consequently, the internal microscopic air–water structures are affected by the turbulence intensity of both the macroscopic entire flow and the microscopic specific air quantity.

Because of the significant difference in microscopic air–water structure between the high and low self-aerated regions, the mean cross-sectional air chord length is separately defined as $(D_{mean})_H$ and $(D_{mean})_L$, demarcated by y_{50}.

High aerated region:

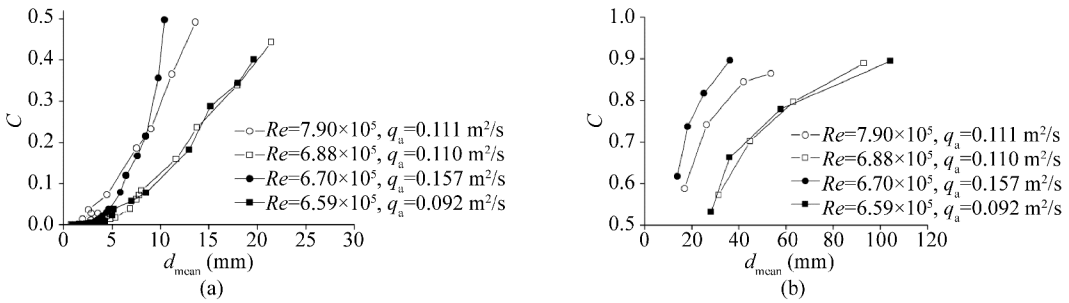

Fig. 7. Mean air chord length d_{mean} distributions in (a) low and (b) high self-aerated area.

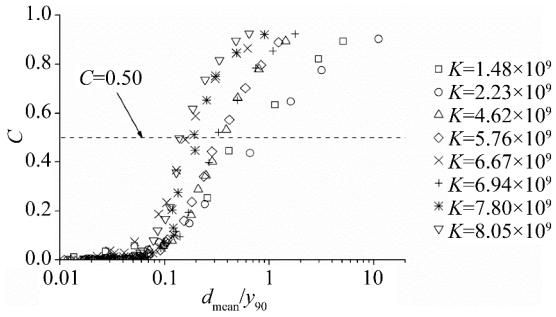

Fig. 8. Effect of K on the d_{mean}/y_{90} distribution in the self-aerated region.

$$(D_{mean})_H = \frac{1}{y_{90}-y_{50}}\int_{y_{50}}^{y_{90}} d_{mean}(y)dy; \quad (7)$$

Low aerated region:

$$(D_{mean})_L = \frac{1}{y_{50}-y_0}\int_{y_0}^{y_{50}} d_{mean}dy. \quad (8)$$

The effects of the coefficient K on $(D_{mean})_L$ and $(D_{mean})_H$ are shown in Fig. 9. To derive the relationship between D_{mean}/y_{90} and K, data from Chanson and Cummings (1995) and Zhang et al. (2008) are considered. The self-aerated flow Re and C_{mean} expand to 9.6×10^5 and 0.45, respectively. With an approximately two orders of magnitude increase in K, the air chord length decreases approximately by one order of magnitude, following the power approximation:

$$\frac{(D_{mean})_H}{y_{90}} = mK^{-0.5}, \quad 1.49\times10^9 \leqslant K \leqslant 3.07\times10^{11}; \quad (9)$$

$$\frac{(D_{mean})_L}{y_{90}} = nK^{-0.5}, \quad 1.49\times10^9 \leqslant K \leqslant 3.07\times10^{11}, \quad (10)$$

where $m = 9\times10^3$ and $n = 9\times10^2$ are the coefficients for the high and low self-aerated regions, respectively, derived from data analysis. Moreover, the length scale of the entrained air in the high-aeration region is in an order of magnitude larger than that in the low aeration region, and the difference remains throughout.

In terms of the air count rate, the effect of the coefficient K on the maximum air count rate at the flow cross-section F_{max} is shown in Fig. 10. The maximum F_{max} is normalized as $F_{max}\cdot y_{90}/V$. This data analysis indicates that with the increase of coefficient K, the air bubble count increases.

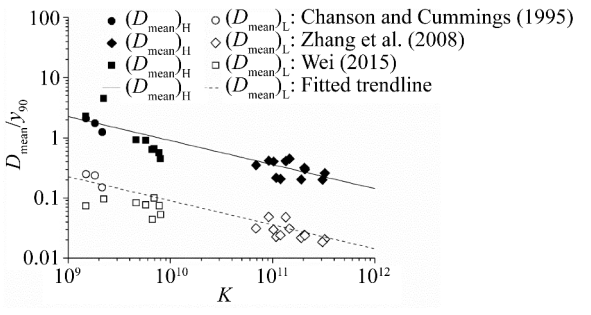

Fig. 9. $(D_{mean})_H/y_{90}$ and $(D_{mean})_L/y_{90}$ with the increasing trend of K.

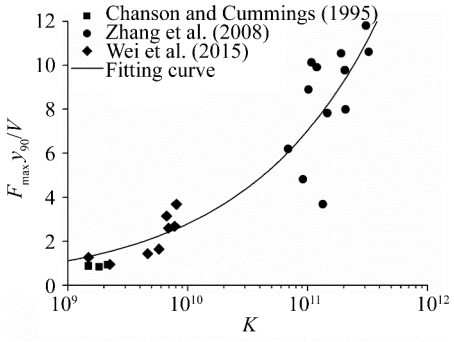

Fig. 10. Effect of K on $F_{max}y_{90}/V$.

This gradient is generally large, following the power approximation:

$$\frac{F_{max}y_{90}}{V} = 2.8\times10^{-4}\cdot K^{0.4}, \quad 1.49\times10^9 \leqslant K \leqslant 3.07\times10^{11}. \quad (11)$$

5 Analyses and discussions

5.1 Interior transition interface of air–water structure

The transition interface hypothesis has been proposed in the theoretical calculation model of the air concentration distribution in self-aerated flows. The measurement test and observation of self-aerated flows show the significant difference in air–water structure at the air–water flow cross-section, including individual air bubbles, large-scaled spray and cluster, free surface deformation and water droplets (Straub and Anderson, 1958; Wu, 1988; Wei et al., 2015). For individual air bubbles diffusing in water flows, the theoretical analysis (Lin and Gong, 1962) based on the one-dimensional turbulence exchange developed the diffusion equation as:

$$u_r C\cos\theta - K\left(\frac{1-2C}{1-C}\right)\frac{dC}{dy} = 0, \quad (12)$$

where u_r is the bubble rise velocity, θ is the channel slope, and K is the turbulent diffusion coefficient. The fluctuations of air concentration, density and bubble rise fluctuations accompanied with the flow turbulence fluctuation were considered. In Fig. 11, the critical breaking point of air concentration is $C = 0.50$ for the theoretical momentum transfer in air–water flows. When the local air concentration exceeds 0.50, the form of the air–water structure as the carrier of air–water momentum transfer changes from individual air bubbles to other structures, such as spray, clusters, and water droplets. Thus, it is reasonable to consider the characterized flow depth y_{50} as the interior transition interface of the air–water structure in self-aerated flows. In addition, compared with the theoretical air concentration distribution profiles of self-aerated flows, the breaking point exists when the aeration level is relatively low (C_{mean}<0.50), indicating that the interior transition interface of the air–water structure always remains in the flow cross-section. When the aer-

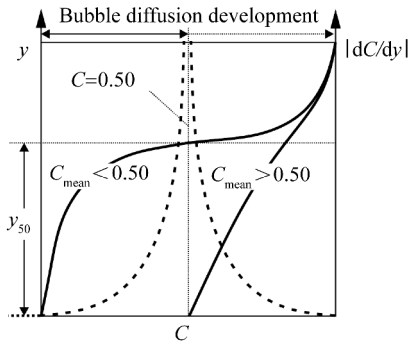

Fig. 11. Comparison between theoretical air concentration distribution (solid line) and gradient profiles (dashed line).

ation level improves, the y_{50} moves toward the channel bottom, and the effect of the interior transition interface gets weak. The air concentration gradient profile finally gets back to the continuous curve for strong aeration (C_{mean}> 0.50), indicating that the turbulence transfer in the air–water flow occurs as air bubble transport. Consequently, y_{50} is the macroscopic parameter with specific microscopic property, and it is reasonable to classify and represent the interior development process of the air–water mixture on the basis of y_{50}.

5.2 Scale effect of microscopic air–water structure

Based on recent engineering practices, the local quantity and size of microscopic air bubbles are the two key parameters for aeration and cavitation erosion protection (Wu et al., 2017). A high count rate of small air bubbles can make a good contribution to avoiding cavitation erosion (Chen et al., 2003), even for the local air concentration lower than the traditional criterion for cavitation erosion protection (Russell and Sheehan, 1974). The present analysis of the air-water flows shows that the air chord length is smaller with larger air count rate for larger air quantity with other conditions identical. When the air quantity and Reynolds number of prototype self-aerated open-channel flows are much larger compared with the scaled physical model and that the total air entrainment (the sum of entrained air and entrapped air) further increases with flow Reynolds number (Wei et al., 2016), it is difficult to achieve air quantity similarity. This results in difficulty to scale the relationship between macroscopic air concentration and microscopic air–water properties. For a prototype case in the Xiaolangdi discharge tunnel chute flow (Liang et al., 2002), the coefficient K of the prototype air–water flow was approximately 10^3–10^4 orders of magnitude larger than that of the physical model. Assuming that the mean cross-sectional air concentration is approximately identical, this may lead to the decrease of the tiny-air-bubble size (air chord length smaller than 4 mm) proportion by approximately 65.9% between the prototype and the model measurement. The scale effects of the entrained air bubble size and the amount of air–water flow are hardly reduced, resulting in the scale effect of the microscopic air–water mixture. Small interactions between air and water entities cannot be accurately scaled, and the particle number reduces and the size of the particle gets larger in the scaled model compared with the prototype, even with a large-scaled model and limitations with some critical requirements (Felder and Chanson, 2017). Thus, it is necessary to develop a new theoretical model of microscopic air–water structure prediction based on air entrainment and bubble diffusion mechanisms and to promote research of aeration and cavitation erosion protection.

5.3 Self-similarity relationship

This study shows a link between macroscopic and microscopic air–water properties, confirming that the microscopic air chord length and count rate are strongly affected by the macroscopic flow Reynolds number and air quantity. The analysis was conducted in a different experimental facility and with different instrumentation. The sensor size and the specific threshold value affect the measurable sizes and, particularly, the air chord length and air count rate, resulting in some variations in the microscopic air–water properties of self-aerated flows. However, the agreement demonstrates a wide spectrum use, including the developing and fully developed self-aerated regions, based on a large number of data analyses. Eqs. (4)–(5) and Eqs. (9)–(11) depict a series of self-similarity relationships between interior air–water structures and the corresponding macroscopic mixture flow conditions. For the macroscopic characterized flow depth, the well fit correlation between y_{50}/y_{90} and C_{mean} is obtained in both the model and the prototype self-aerated open-channel flows, independent of chute slope and such flow conditions as Froude number and Reynolds number. Moreover, the mean cross-sectional air chord length and air count rate can be directly related to the macroscopic flow Reynolds number and air quantity.

In further research on the detailed air–water properties, it is necessary to pay more attention to the mechanism of air entrainment in free-surface open-channel flows, developing the theory and method about quantitative prediction of air concentration and air quantity. Prototype scale experiments are needed to verify and apply the present approach. Moreover, because the complex air–water structure information is closely linked to the flow micro-turbulence dynamics, it is strongly recommended that the air bubble scale and kinematic characteristics should be investigated directly and in detail.

6 Conclusions

An analytical comparison of interior air–water mixture characteristics affected by the relationship between microscopic and macroscopic air–water properties was conducted, focusing on the self-aerated open-channel flows. A series of experimental and prototype tests were conducted including

those in both self-aerated developing and equilibrium regions. The characterized flow depth y_{50} describing the self-aeration development process was discussed. The effects of flow Reynolds number and air quantity on microscopic air chord length and count rate were investigated. The following conclusions can be drawn.

As self-aeration of open-channel flow develops with the increase of mean air concentration, the characterized flow depth y_{50} distinguishes the process as two different linear trends with a breaking point at $C_{mean} = 0.50$. Based on a series of systematic comparisons of air count rate and chord size, the y_{50} is a specific criterion to distinguish the development process of interior air–water mixture. Both flow Reynolds number and air quantity in self-aerated regions influence the microscopic air bubble size scale and count rate. For identical mean cross-sectional air concentration, the air count rate increases, and the proportion of the small air chord length improves for larger flow Reynolds number and larger air discharge per unit width, with a decrease of mean air chord length in the high and low self-aerated regions. The coefficient $K=Re\cdot q_a/v$, considering both the macroscopic flow turbulence and the air quantity, describes microscopic air–water structure differences in self-aerated flows. A series of self-similarity relationships exist between K and the mean air chord length and air count rate.

Because of the link between macroscopic and microscopic air–water properties in self-aerated air–water flows, the microscopic air–water structures, including air size and count rate, cannot be accurately scaled to prototype through scale-physical experiments, even for the identical macroscopic flow conditions. It is necessary to pay more attention to the air entrainment and bubble diffusion mechanisms in self-aerated open-channel flows in the further research.

References

Afshar, N.R., Asawa, G.L. and Raju, K.G.R., 1994. Air concentration distribution in self-aerated flow, *Journal of Hydraulic Research*, 32(4), 623–631.

Anderson, A.G., 1955. *The Distribution of Air in Self-Aerated Flow in A Smooth Open Channel*, Report No.48, University of Minnesota, Minneapolis, USA.

Boes, R.M. and Hager, W.H., 2003. Two-phase flow characteristics of stepped spillways, *Journal of Hydraulic Engineering*, 129(9), 661–670.

Brocchini, M. and Peregrine, D.H., 2001a. The dynamics of strong turbulence at free surfaces. Part 1. Description, *Journal of Fluid Mechanics*, 449(1), 225–254.

Brocchini, M. and Peregrine, D.H., 2001b. The dynamics of strong turbulence at free surfaces. Part 2. Free-surface boundary conditions, *Journal of Fluid Mechanics*, 449(1), 255–290.

Cain, P., 1978. *Measurements Within Self-Aerated Flow on A Large Spillway*, Ph. D. Thesis, University of Canterbury, Christchurch, New Zealand.

Cain, P. and Wood, I.R., 1981. Measurements of self-aerated flow on a spillway, *Journal of the Hydraulics Division*, 107(11), 1425–1444.

Chanson, H., 1995. Air *Bubble Entrainment in Free-Surface Turbulent Flows*: *Experimental Investigations*, Report Ch46/95, University of Queensland, Brisbane, Australia.

Chanson, H., 2002. *The Hydraulics of Stepped Chutes and Spillways*, Balkema, Lisse, The Netherlands.

Chanson, H. and Cummings, P.D., 1995. *Air–Water Interface Area in Supercritical Flows Down Small-Slope Chutes*, Report Ce151, University of Queensland, Brisbane, Australia.

Chanson, H., 2007. Hydraulic engineering in the 21st century: Where to? 13th Arthur Ippen awardee, IAHR member *Journal of Hydraulic Research*, 45(3), 291–301.

Chanson, H., 2013. Hydraulics of aerated flows: qui pro quo? *Journal of Hydraulic Research*, 51(3), 223–243.

Chen, X.P., Xi, R.Z., Shao, D.C. and Liang, B., 2003. New concept of air entrainment effect on mitigating cavitation damage, *Journal of Hydraulic Engineering*, 34(8), 70–74. (in Chinese)

Deng, J., Wei, W.R., Xu, W.L., Tian, Z. and Zhang, F.X., 2015. Experimental study on air-phase frequency in self-aerated flow, *Proceedings of the Institution of Civil Engineers – Water Management*, 168(4), 153–161.

Felder, S. and Chanson, H., 2016. Air–water flow characteristics in high-velocity free-surface flows with 50% void fraction, *International Journal of Multiphase Flow*, 85, 186–195.

Felder, S. and Chanson, H., 2017. Scale effects in microscopic air-water flow properties in high-velocity free-surface flows, *Experimental Thermal and Fluid Science*, 83, 19–36.

Ferrando, A.M. and Rico, J.R., 2002. On the incipient aerated flow in chutes and spillways, *Journal of Hydraulic Research*, 40(1), 95–97.

Gulliver, J.S. and Rindels, A.J., 1993. Measurement of air-water oxygen transfer at hydraulic structures, *Journal of Hydraulic Engineering*, 119(3), 327–349.

Hager, W.H., 1991. Uniform aerated chute flow, *Journal of Hydraulic Engineering*, 117(4), 528–533.

Hall, L.S., 1943. Entrainment of air in flowing water: a symposium: open channel flow at high velocities, *Transactions of the American Society of Civil Engineers*, 108(1), 1393–1434.

Heller, V., 2011. Scale effects in physical hydraulic engineering models, *Journal of Hydraulic Research*, 49(3), 293–306.

Killen, J.M., 1968. *The Surface Characteristics of Self-aerated Flow in Steep Channels*, Ph. D. Thesis, University of Minnesota, Minneapolis, USA.

Liang, B., Chen, X.P., Shao, D.C. and Cai, H., 2002. Air bubble gradation of high velocity aerated flow, *Hydro-Science and Engineering*, (2), 66–68. (in Chinese)

Lin, B.N. and Gong, Z.Y., 1962. On some properties of aerated flow in open channels, *Journal of Hydraulic Engineering*, (1), 8–15. (in Chinese)

Pfister, M. and Chanson, H., 2014. Two-phase air-water flows: Scale effects in physical modeling, *Journal of Hydrodynamics*, *Ser. B*, 26(2), 291–298.

Russell, S.O. and Sheehan, G. J., 1974. Effect of entrained air on cavitation damage, *Canadian Journal of Civil Engineering*, 1(1), 97–107.

Rutschmann, P. and Hager, W.H., 1990. Air entrainment by spillway aerators, *Journal of Hydraulic Engineering*, 116(6), 765–782.

Schultz, M.P. and Flack, K.A., 2013. Reynolds-number scaling of turbulent channel flow, *Physics of Fluids*, 25(2), 025104.

Straub, L.G. and Anderson, A.G., 1958. Experiments on self-aerated flow in open channels, *Journal of the Hydraulics Division*, 84(7), 1–35.

Takahashi, M. and Ohtsu, I., 2012. Aerated flow characteristics of skimming flow over stepped chutes, *Journal of Hydraulic Research*,

50(4), 427–434.

Toombes, L. and Chanson, H., 2007. Surface waves and roughness in self-aerated supercritical flow, *Environmental Fluid Mechanics*, 7(3), 259–270.

Valero, D. and Bung, D.B., 2018. Reformulating self-aeration in hydraulic structures: Turbulent growth of free surface perturbations leading to air entrainment, *International Journal of Multiphase Flow*, 100, 127–142.

Volkart, P., 1980. The mechanism of air bubble entrainment in self-aerated flow, *International Journal of Multiphase Flow*, 6(5), 411–423.

Wang, S.K., Lee, S.J., Jones, O.C. and Lahey, R.T., 1990. Statistical analysis of turbulent two-phase pipe flow, *Journal of Fluids Engineering*, 112(1), 89–95.

Wei, W.R., 2015. *Research on Self-Aeration Characteristics in Developing Region of Open Channel Flows*, Ph. D. Thesis, Sichuan University, China. (in Chinese)

Wei, W.R., Deng, J. and Zhang, F.X., 2016. Development of self-aeration process for supercritical chute flows, *International Journal of Multiphase Flow*, 79, 172–180.

Wei, W.R., Deng, J., Zhang, F.X. and Tian, Z., 2015. A numerical model for air concentration distribution in self-aerated open channel flows, *Journal of Hydrodynamics*, *Ser. B*, 27(3), 394–402.

Wilhelms, S.C., 1997. *Self-Aerated Spillway Flow*, Ph. D. Thesis, University of Minnesota, Minneapolis, USA.

Wilhelms, S.C. and Gulliver, J.S., 2005. Bubbles and waves description of self-aerated spillway flow, *Journal of Hydraulic Research*, 43(5), 522–531.

Wood, I.R., 1983. Uniform region of self-aerated flow, *Journal of Hydraulic Engineering*, 109(3), 447–461.

Wu, C.G., 1988. A research on self-aerated flow in open channels, *Journal of Hydroelectric Engineering*, (4), 23–36. (in Chinese)

Wu, J.H., Su, K.P., Wang, Y. and Guo, W.J., 2017. Effect of air bubble size on cavitation erosion reduction, *Science China Technological Sciences*, 60(4), 523–528.

Xi, R.Z., 1988. Characteristics of self-aerated flow on steep chutes, *Proceedings of International Symposium on Hydraulics for High Dams*, IAHR, Beijing, China.

Zhang, F.X., Xu, W.L., Deng, J., Gang, L. and Gao, P., 2008. Distribution of the bubble chord length and numbers in self-aerated open channel flows, *Journal of Hydroelectric Engineering*, 27(1), 53–57. (in Chinese)